ACSNANO

www.acsnano.org

ARTICLE

Separable Microneedle Patch to Protect and Deliver DNA Nanovaccines Against COVID-19

Yue Yin, Wen Su, Jie Zhang, Wenping Huang, Xiaoyang Li, Haixia Ma, Mixiao Tan, Haohao Song, Guoliang Cao, Shengji Yu, Di Yu, Ji Hoon Jeong, Xiao Zhao, Hui Li,* Guangjun Nie,* and Hai Wang*

Cite This: https://doi.org/10.1021/acsnano.1c03252

Read Online

ACCESS | Metrics & More | Article Recommendations | Supporting Information

ABSTRACT: **The successful control of coronavirus disease 2019 (COVID-19) pandemic is not only relying on the development of vaccines, but also depending on the storage, transportation, and administration of vaccines. Ideally, nucleic acid vaccine should be directly delivered to proper immune cells or tissue (such as lymph nodes). However, current developed vaccines are normally treated through intramuscular injection, where immune cells do not normally reside. Meanwhile, current nucleic acid vaccines must be stored in a frozen state that may hinder their application in developing countries. Here, we report a separable microneedle (SMN) patch to deliver polymer encapsulated spike (or nucleocapsid) protein encoding DNA vaccines and immune adjuvant for efficient immunization. Compared with intramuscular injection, SMN patch can deliver nanovaccines into intradermal for inducing potent and durable adaptive immunity. IFN-γ^+CD4/8$^+$ and IL-2$^+$CD4/8$^+$ T cells or virus specific IgG are significantly increased after vaccination. Moreover, *in vivo* results show the SMN patches can be stored at room temperature for at least 30 days without decreases in immune responses. These features of nanovaccines-laden SMN patch are important for developing advanced COVID-19 vaccines with global accessibility.**

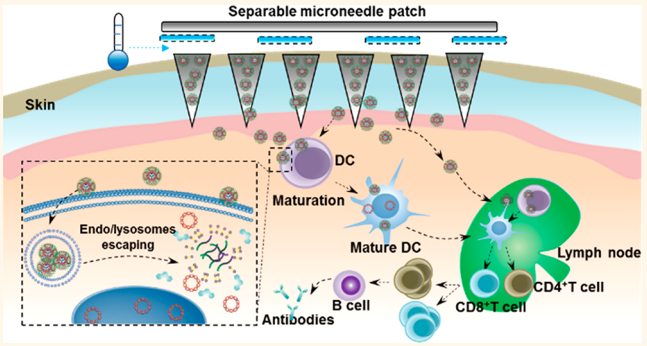

KEYWORDS: *COVID-19, DNA vaccines, immune adjuvant, separable microneedle, adaptive immunity*

The coronavirus disease 2019 (COVID-19) has caused more than 123 million infections in 219 countries or territories with more than 2.7 million deaths (World Health Organization, WHO) as of 23 March 2021.[1] Effective vaccines against severe acute respiratory syndrome coronavirus 2 (SARS-CoV-2) are urgently needed to reduce the enormous burden of mortality and morbidity. Due to the safety, humoral and cellular immune response, and ease of designing and manufacturing, nucleic acid vaccines (DNA or RNA) have been investigated to generate virus proteins in antigen-presenting cell (APC), which mimic SARS-CoV-2 antigens to stimulate the immune response.[2−4] To date, more than 170 COVID-19 vaccines are under development or undergoing human clinical trials, while three vaccines (Pfizer-BioNTech, Moderna, and Johnson & Johnson's Janssen COVID-19 vaccines) have been authorized by the U.S. Food and Drug Administration (FDA) for emergency use.[5] However, those vaccines always require storage conditions during manufacturing, shipping, and the end-user site. According to those manufacturers, they may be stable in a frozen state for several months, but only for several hours at room temperature.[6] Unfortunately, many less-developed or developing countries have insufficient facilities for temperature-controlled shipping and storage facilities for immunization.[7] Meanwhile, a shortage of healthcare workers should also be noted in those countries as only professionals can operate current approved vaccines. Of note, it is important to recognize that the COVID-19 pandemic cannot be relieved even if it is just out of control in one region. Collectively, there is an urgent need to establish methods to make COVID-19 vaccines more stable and convenient for immunization.

SARS-CoV-2 is made of four structural proteins, namely spike (S), membrane (M), envelope (E), and nucleocapsid (N) protein.[8] S protein is the main target used for developing SARS-CoV-2 vaccines.[9,10] In contrast, M and E proteins may not be suitable for developing vaccines as studies indicated that

Received: April 18, 2021
Accepted: August 26, 2021

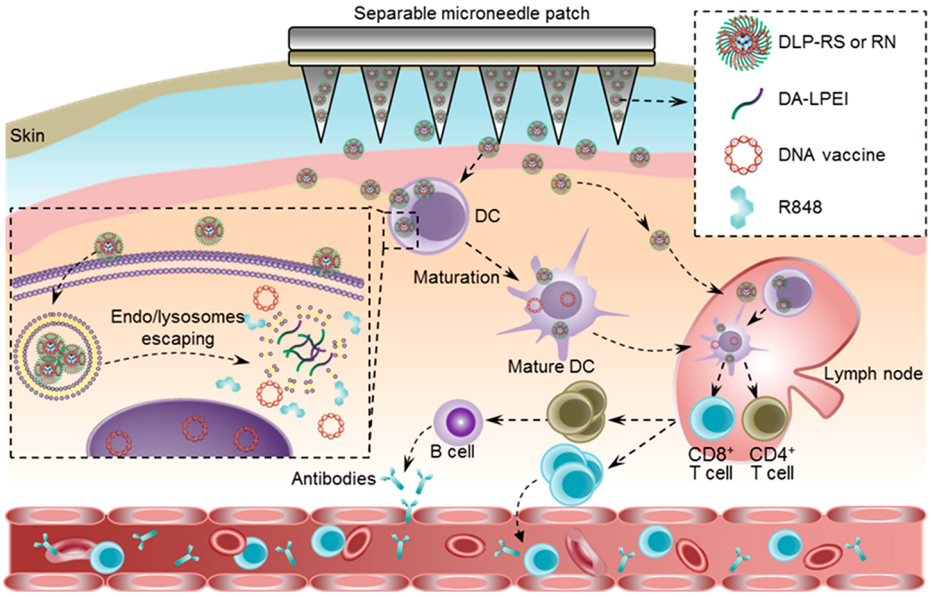

Figure 1. Schematic illustration of separable microneedle patch mediated intracutaneous delivery of DNA nanovaccines for fighting SARS-CoV-2 virus. Deoxycholic acid conjugated low molecular weight polyethylenimines (DA-LPEI) was applied to encapsulate both immunostimulant (R848) and S- or N-protein encoding DNA vaccines (DLP-RS or RN). The microneedle patch can painlessly penetrate the epidermis into the dermis layer, where they release the DLP-RS or DLP-RN nanoparticles. DNA nanovaccines can be uptake by dendritic cells (DCs) or other APCs in dermis layer directly. The DA-LPEI is designed to break the endo/lysosomes and DNA vaccines can be released to generate virus antigens in DCs. Meanwhile, the released nanoparticles could diffuse into the lymph capillaries and move through the lymph flow to lymph nodes, where they could present virus antigens in DCs. The mature DCs could induce SARS-CoV-2 virus-specific CD4/CD8$^+$ T cells. CD8$^+$ T cells can destroy the virus infected cells while CD4$^+$ T cells can provide help to B cells for affinity maturation and antibody production.

they cannot induce strong humoral responses.[11] Development of vaccines with N protein is not well-understood currently even though N protein is the most abundant viral protein and is highly immunogenic.[12] Recombinant DNA technology has revolutionized the development of vaccines against microbial pathogens, thereby creating opportunities to control the current COVID-19 pandemic.[13] However, low efficiency of cellular uptake greatly limits transfection effectiveness of DNA vaccine in APCs.[14,15] To overcome this issue, lipidoid nanoparticles (LNPs) have been developed to deliver DNA vaccines in APCs, but studies have indicated that the LNPs may be unstable at room temperature as a significant amount of them would form aggregation and decrease the transfection efficacy.[16]

Regarding protection for SARS-CoV-2 infection with vaccines, emerging data have demonstrated the importance of both humoral and cellular immunity.[17] It is well-known that generation of neutralizing antibodies is crucial for protecting people from virus infection.[18,19] Importantly, SARS-CoV-2-specific T cell responses have been identified in acute and convalescent COVID-19 patients associated with milder situations, indicating that T cell responses are important for SARS-CoV-2 protection.[20] Therefore, coadministration of immunostimulant with SARS-CoV-2 vaccines may better activate the T cell responses for effective protection. Resiquimod (R848) mimics the pathogen-associated molecular patterns that activate toll-like receptors (TLR) 7/8 and has been used as an immunostimulant in humans against viral infections.[21] However, as a hydrophobic adjuvant, it is crucial to deliver R848 and DNA vaccines (hydrophilic) at right immunological tissues (i.e., lymph nodes) for presenting virus antigens.

To tackle these challenges, we here report a separable microneedle (SMN) patch to deliver polymer encapsulated S- or N-protein encoding DNA vaccines for efficient immunization. Deoxycholic acid conjugated low molecular weight polyethylenimines (LPEI, DA-LPEI) was synthesized to form amphiphilic polymer for encapsulating hydrophobic immunostimulant (Resiquimod, R848) in the core of the nanoparticles (DLP-R, Figure 1). DA-LPEI polymer can efficiently deliver plasmid into cells for gene transfection with minimal cytotoxicity.[22,23] Then, S- or N-protein encoding DNA vaccines were absorbed onto the surface of DLP-R nanoparticles through electrostatic interaction (DLP-RS or DLP-RN, Figure 1). To deliver nanovaccines to APCs enriched location, DLP-RS or DLP-RN nanoparticles were further packaged in SMN patch for intracutaneous injection as skin is an immunologically active tissue.[24,25] The DLP-RS or DLP-RN nanoparticles could continually release from the microneedle and either deliver nanovaccines into dendritic cells (DCs) or targeted deliver DNA nanovaccines to lymph node (Figure 1). Importantly, the DLP nanoparticles could assistant the DNA vaccines escaping from the endo/lysosomes to present the S- or N-protein in DCs. Then, the mature DCs could induce SARS-CoV-2 virus-specific CD4$^+$/CD8$^+$ T cells. CD8$^+$ T cells can destroy the virus infected cells while CD4$^+$ T cells can provide help to B cells for affinity maturation and antibody production (Figure 1).

RESULTS AND DISCUSSION

Preparation and Characterization of DNA Vaccines. PEI is cationic polymer that has been widely used for gene delivery.[26] To encapsulate R848, LPEI was first reacted with deoxycholic acid to form amphiphilic polymers. The successful conjugation of DA-LPEI was confirmed with nuclear magnetic

https://doi.org/10.1021/acsnano.1c03252
ACS Nano XXXX, XXX, XXX−XXX

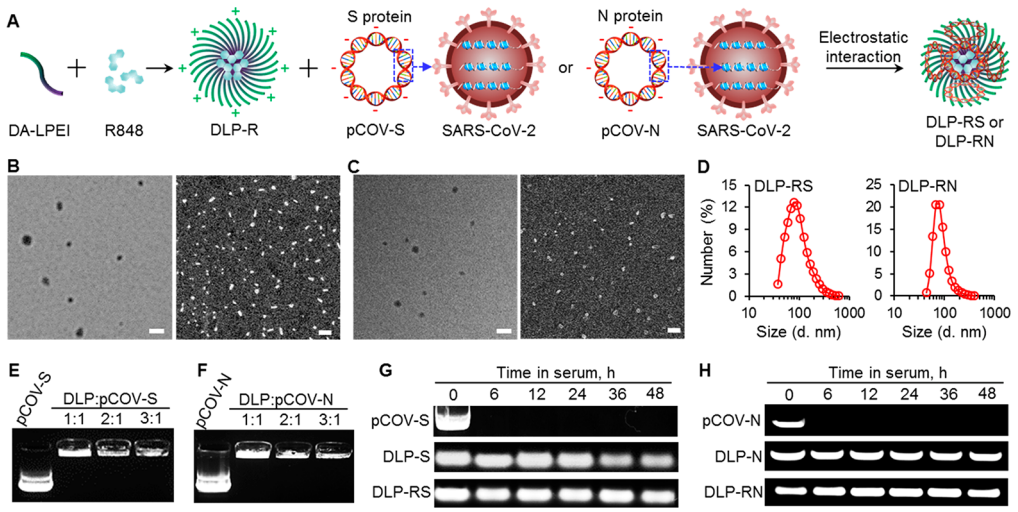

Figure 2. Schematic illustration and characteristics of DNA nanovaccines. (A) DA-LPEI amphiphilic polymer was designed to encapsulate the hydrophobic R848 in the core of nanoparticles (DLP-R) and plasmid DNA for expressing S- or N-protein (pCOV-S or pCOV-N) was absorbed on the nanoparticles through electrostatic interaction (DLP-RS or DLP-RN). (B) Transmission electron microscopy (TEM, left) and scanning electron microscopy (SEM, right) images of DLP-RS and (C) DLP-RN nanoparticles. Scale bar: 300 nm. (D) Size distributions of DLP-RS (left) and DLP-RN (right) nanoparticles determined by DLS at 22 °C. (E) Encapsulation efficacy of DLP nanoparticles to pCOV-S or (F) pCOV-N with various weight ratios via electrophoretic mobility shift assay, showing almost all pCOV-S or pCOV-N were absorbed on the nanoparticles. (G) Stability of free and encapsulated pCOV-S or (H) pCOV-N in DLP-RS in serum at 37 °C for different times, suggesting the pCOV-S or pCOV-N can be efficiently protected after encapsulated in the nanoparticles.

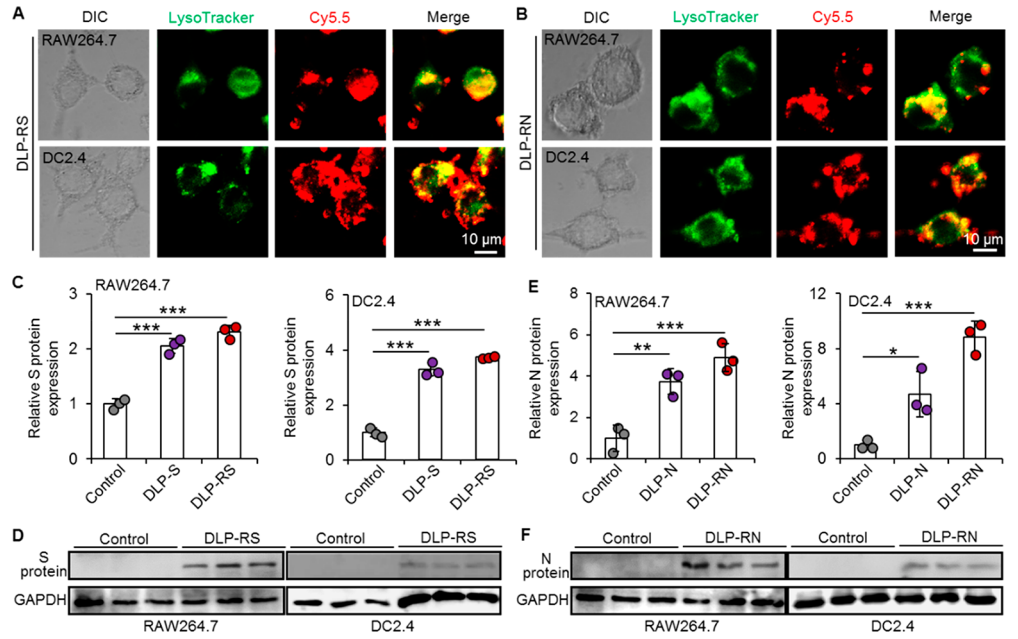

Figure 3. *In vitro* transfection and virus antigen presentation in immune cells. (A) Cellular uptake and endo/lysosome escaping of DLP-RS and (B) DLP-RN treated RAW264.7 and DC2.4 cells for 4 h at 37 °C. The pCOV-S or pCOV-N was labeled with Cy5.5 (red) and the endo/lysosomes were stained using LysoTracker Green (green). DIC, differential interference contrast. (C) Evaluations of S protein expression in RAW264.7 and DC2.4 cells 48 h after DLP-RS (2 μg/mL for pCOV-S) transfections via ELISA and (D) Western blot. Those results show the successful presentation of S protein in both RAW264.7 and DC2.4 cells. Error bars represent ± SD (n = 3). (E) Evaluations of N-protein expression in RAW264.7 and DC2.4 cells 48 h after DLP-RN transfections via ELISA and (F) Western blot. Error bars represent ± SD (n = 3). *P < 0.05, **P < 0.01, ***P < 0.001 (ANOVA analysis with multiple comparisons).

resonance (NMR) spectra as shown in Supporting Information (SI) Figure S1. This is further confirmed with Fourier-transform infrared (FTIR) spectroscopy. FTIR spectra of DA-LPEI exhibit absorption bands corresponding to amide bond, suggesting the successful reaction between deoxycholic acid and LPEI (SI Figure S2). Next, hydrophobic R848 and DA-LPEI were mixed and assembled to form the "oil-in-water" nanostructures,[27] whereas the R848 was encapsulated in the core of nanoparticles (Figure 2A). Plasmid encoding S- or N-protein (pCOV-S or pCOV-N, SI Figure S3) were then decorated on the surface of DLP-R nanoparticles through electrostatic interaction (DLP-RS or DLP-RN, Figure 2A). Transmission electron microscopy (TEM, left) and scanning electron microscopy (SEM, right) images of DLP-RS and

https://doi.org/10.1021/acsnano.1c03252
ACS Nano XXXX, XXX, XXX−XXX

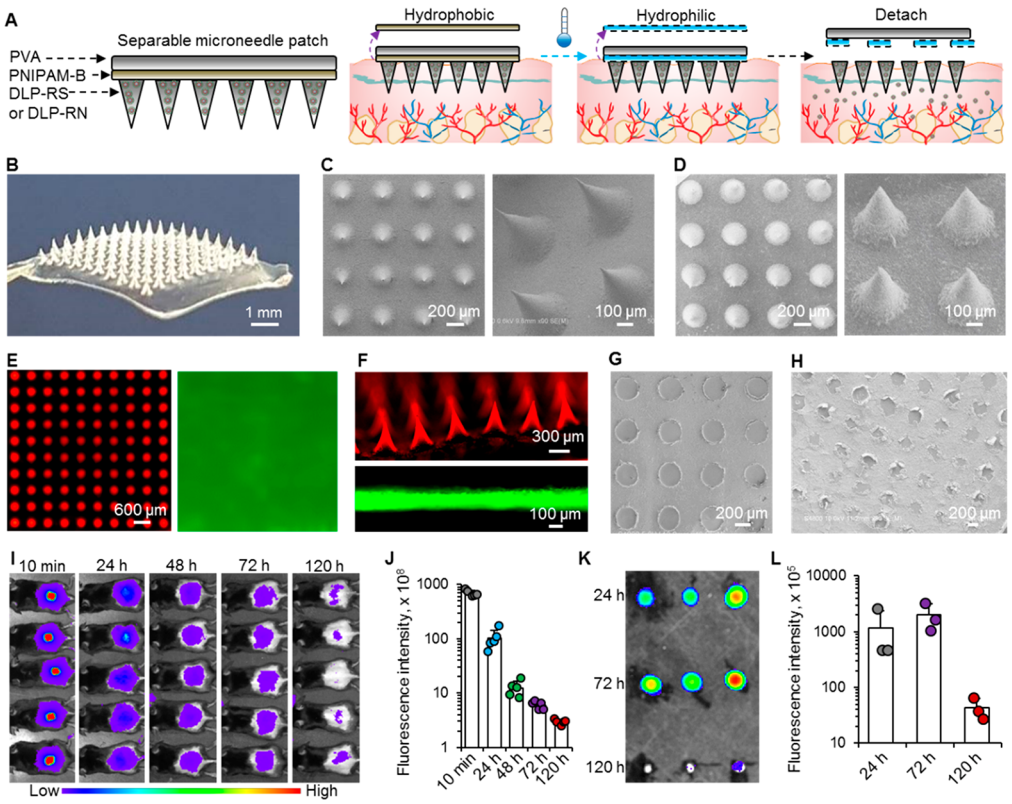

Figure 4. Schematic illustration and characterizations of SMN patches. (A) The thermal responsive PNIPAM-B polymer was inserted between the backing layer (top part, PVA) and microneedles containing DLP-RS or DLP-RN. The PNIPAM-B polymer is hydrophobic at room temperature and transfers to hydrophilic if the temperature is lower than LCST (14−16 °C). Using this property, the backing layer of SMN can be easily separated from skin and leave the microneedles in the skin. (B) A photograph of a whole microneedle patch. (C) SEM images of SMN patch or (D) DNA nanovaccines-laden SMN patch (SMN-DLP-RS), showing the rough surface of microneedles after packaged with nanovaccines. (E) Typical fluorescence images of SMN-DLP-RS patch (top view) using ChemiDoc Touch Imaging System. The red fluorescence of nanovaccines (Cy5.5) is only observable in the microneedle while green fluorescence (PNIPAM-B mixed with FITC) is uniformly distributed under the microneedle. (F) Side view of SMN-DLP-RS patch further confirming the distribution of nanovaccines and PNIPAM-B in the SMN patch. (G) SEM images of SMN patches after incubated in cold water (~13 °C) for 3 min, showing those microneedles have separated from the backing layer. (H) SEM images of SMN patches after manually pressing in the skin of C57BL/6 mice. The patch has been cooled with cold water in bottle (~13 °C) for 3 min. (I) IVIS imaging and (J) quantitative fluorescence intensity of mice after inserted microneedles containing Cy5.5-DNA nanovaccines in skin for different times. Error bars represent ± SD (n = 5). (K) IVIS imaging and (L) quantitative fluorescence intensity of Cy5.5-DNA nanovaccines in lymph nodes after treated for 24, 72, and 120 h. Error bars represent ± SD (n = 3).

DLP-RN nanoparticles are given in Figure 2B,C, respectively, showing the DLP-RS and DLP-RN nanoparticles are well dispersed with a spherical morphology. We further checked the average size of the DLP-RS and DLP-RN nanoparticles in deionized water using dynamic light scattering (DLS) to be ~85 nm and ~75 nm in diameter, respectively (Figure 2D). The size of DLP-RS nanoparticles is slightly larger than DLP-RN, which is probably due to the larger size of pCOV-S (9269 bp) than pCOV-N (6734 bp).

We next investigated the protecting capability of DLP-RS or DLP-RN nanoparticles. As shown in Figure 2E,F, migration of the pCOV-S or pCOV-N into the agarose gel was completely prevented after incubated with DLP nanoparticles, indicating DNA vaccines can be efficiently absorbed on the DLP nanoparticles. This is further confirmed with the surface zeta potential of DLP-R and DLP-RS or DLP-RN nanoparticles. As shown in SI Figure S4, the zeta potential of DLP-RS (or RN) nanoparticles decreased to ~14.7 mV after modifying them with negatively charged DNA vaccines, suggesting DNA vaccines were successfully decorated on the DLP-R nanoparticles. The capability of DLP nanoparticles in protecting DNA vaccines was tested in serum with various incubation time. Naked pCOV-S or pCOV-N disappeared in serum less than 6 h because of the degradation (Figure 2G,H). In contrast, those DNA vaccines in DLP-RS or DLP-RN nanoparticles were observable even after incubated in serum for 48 h, confirming the DNA vaccines can be protected with DLP nanoparticles from degradation (Figure 2G,H).

Transfection and Virus Antigen Presentation *In Vitro*.

Although PEI has been widely studied for gene delivery, the cytotoxicity of PEI is a great concern for potential application.[28] Studies have suggested that the toxicity of PEI can be decreased by reducing its molecular weight, but the transfection efficacy of LPEI is low.[29] To address this issue, DA-LPEI was applied in this study to enhance its transfection efficacy.[22,23] Two types of APCs (RAW264.7 and DC2.4) were used for the *in vitro* experiments. First, we examined the cytotoxicity of DA-LPEI and the prepared nanoparticles. As shown in SI Figure S5, the toxicities of free DA-LPEI, pCOV-S-laden DLP nanoparticles (DLP-S), or DLP-RS nanoparticles are minimal with various concentrations compared with

https://doi.org/10.1021/acsnano.1c03252
ACS Nano XXXX, XXX, XXX−XXX

control groups. It is worth noting that the immunostimulant (R848) is also not toxic to both RAW264.7 and DC2.4 cells.

Next, the endo/lysosome escaping capability of DLP nanoparticles was investigated by labeling pCOV-S and pCOV-N with fluorescence dye (Cy5.5). The pCOV-S- or pCOV-N-laden nanoparticles were cultured with both RAW264.7 and DC2.4 for 2, 4, or 6 h. As shown in Figure 3A,B and SI Figure S6, the red fluorescence of Cy5.5 partially overlaps with the green fluorescence of LysoTracker Green that stains the endo/lysosomes, suggesting both cells uptake the nanoparticles through endocytosis. Meanwhile, the fluorescence intensity in cells become stronger after cultured for 6 h (Figure 3A,B and SI Figure S6). This is further confirmed with the flow cytometry. As shown in SI Figure S7, cellular uptake of DLP-RS or DLP-RN nanoparticles was significantly increased after cultured with nanoparticles for 6 h. Importantly, a great degree of red fluorescence is not overlapped with green fluorescence, indicating successful escape of the pCOV-S and pCOV-N from endo/lysosomes (Figure 3A,B and SI Figure S6). In contrast, almost no red fluorescence can be detected if incubated the free plasmid with RAW264.7 and DC2.4 cells directly (SI Figure S8), indicating the importance of using DLP nanoparticles.

Having confirmed the endo/lysosome escaping capability, the expression of S- and N-protein in both RAW264.7 and DC2.4 was confirmed with both enzyme-linked immunosorbent assay (ELISA) and Western blot. As shown in Figure 3C, the absorbance of DLP-S or DLP-RS treated RAW264.7 and DC2.4 cells is significantly higher than nontreated cells. This can be further confirmed with the Western blot data as shown in Figure 3D. The data of triplication show that the S proteins were highly expressed in DLP-RS treated RAW264.7 and DC2.4 cells (Figure 3D). Similarly, the existence of N-protein in pCOV-N-laden DLP (DLP-N) or DLP-RN nanoparticles treated cells is confirmed with the higher absorbances than control group according to the ELISA results (Figure 3E). The band of N protein can be also observed in the Western blot images (Figure 3F). However, the band of S- or N-protein cannot be detected if incubated free plasmid (pCOV-S or pCOV-N) with RAW264.7 and DC2.4 cells (SI Figure S9a). Similarly, ELISA results showed that the expressions of S- and N-protein were similar as PBS treated RAW264.7 and DC2.4 cells, indicating the free plasmid treatment cannot express the encoded proteins in immune cells (SI Figure S9b). The transfection capacity of DLP nanoparticles was further confirmed with green fluorescent protein (GFP) encoding plasmid. As shown in SI Figure S10, strong green fluorescence can be detected in GFP plasmid-laden DLP (GLP-G) or DLP-R (DLP-RG) nanoparticles treated cells. The above mentions results indicate that DLP nanoparticles are not toxic to cells and can successfully help the DNA vaccines escaping from endo/lysosome to present the virus antigens in APCs.

Preparation and Characterization of SMN Patch. The successful control of the COVID-19 pandemic is not only relying on the development of vaccines, but also depending on the storage, transportation and administration of the vaccines. Recent approved SARS-CoV-2 vaccines are treated through intramuscular injection, which need health care professionals for operation and may cause blood-related side effects.[30] Ideally, for effective vaccination, the vaccine should be delivered directly to immune cells or proper tissue (such as lymph node). However, immune cells do not normally reside in the muscle tissue. Compared with muscle tissue, skin is an ideal site for immunization as which has an abundance of APCs and immune accessory cells for inducing potent and durable adaptive immunity.[24] Although studies have demonstrated the benefit of intradermal injection of vaccines, it is difficult to achieve a precise and reproducible delivery to the intradermal layer using traditional methods.

To address those limitations, SMN patch was developed to deliver DNA vaccines-laden nanoparticles to intradermal layer for effective vaccination (Figure 4A). Different strategies have been developed to prepare the separable microneedles. For example, sodium bicarbonate and citric acid have been encapsulated in the separating layer to form carbon dioxide bubbles, which could detach the backing layer from microneedles.[31] In another method, the sharp microneedles were mounted on blunt metal shafts. After inserting into the skin, the blunt metal shafts can be separated from the microneedles and left in the skin.[32] Other studies have applied dissolvable polymer as the backing layer to separate from the microneedles.[33] The backing layer can be efficiently detached from the microneedles using those methods, but the separation is not controllable. The separation process would start immediately once the patch is pushed into skin. In this study, we aimed to control the separation with external stimulus and therefore used PNIPAM-B as the separating layer by controlling the skin temperature. SMN patch is composed of a polyvinyl acetate (PVA) and can painlessly penetrate the epidermis into the dermis layer, where they release the DLP-RS or DLP-RN nanoparticles (Figure 4A). Since PVA cannot dissolve in a liquid solution immediately, it is necessary to rapidly separate the backing layer from SMN patch to keep the embedded microneedle in the dermis layer. Thus, we have designed a separating layer between the backing layer and microneedles as shown in Figure 4A. This separating layer was made of poly(*N*-isopropylacrylamide-*co*-butyl acrylate) (PNIPAM-B, NIPAM:B = 8:1, Mn = 30 000), which is a thermally responsive polymer with a lower critical solution temperature (LCST) of 14−16 °C. This means the polymer is insoluble in water (hydrophobic) at room temperature (~22 °C), while it is highly soluble in water (hydrophilic) at or below 14 °C. Therefore, the backing layer can be easily separated from skin by decreasing the temperature of skin to 14−16 °C for several minutes (Figure 4A).

The procedure to fabricate SMN patch is shown in SI Figure S11, which consists of a 10 × 10 array of sharp and conical shape microneedles (Figure 4B). The height of the microneedle is ~600 μm, whereas the bottom radius is ~150 μm. Compared with pure PVA microneedle (Figure 4C), the surface of microneedle has an uneven or irregular surface after loaded DLP-RS or DLP-RN nanoparticles according to the SEM images (Figure 4D). To confirm the positions of nanovaccines and separating layer, we further applied Cy5.5-labeled DNA vaccines and fluorescein isothiocyanate (FITC) mixed PNIPAM-B to fabricate the SMN patch. As shown in Figure 4E,F (for top view and side view, respectively), DNA vaccines-laden nanoparticles can only be observed in the microneedles, whereas the PNIPAM-B is uniformly distributed next to microneedle and formed a single layer. Then, we assessed the skin penetration capability of SMN patch by encapsulating FITC in the microneedles as shown in SI Figure S12a. The successful insertion can be observed in the fluorescence images of skin after removed the backing layer. The is further confirmed with the histological analysis (hematoxylin and eosin, H&E staining). As shown in SI

https://doi.org/10.1021/acsnano.1c03252
ACS Nano XXXX, XXX, XXX−XXX

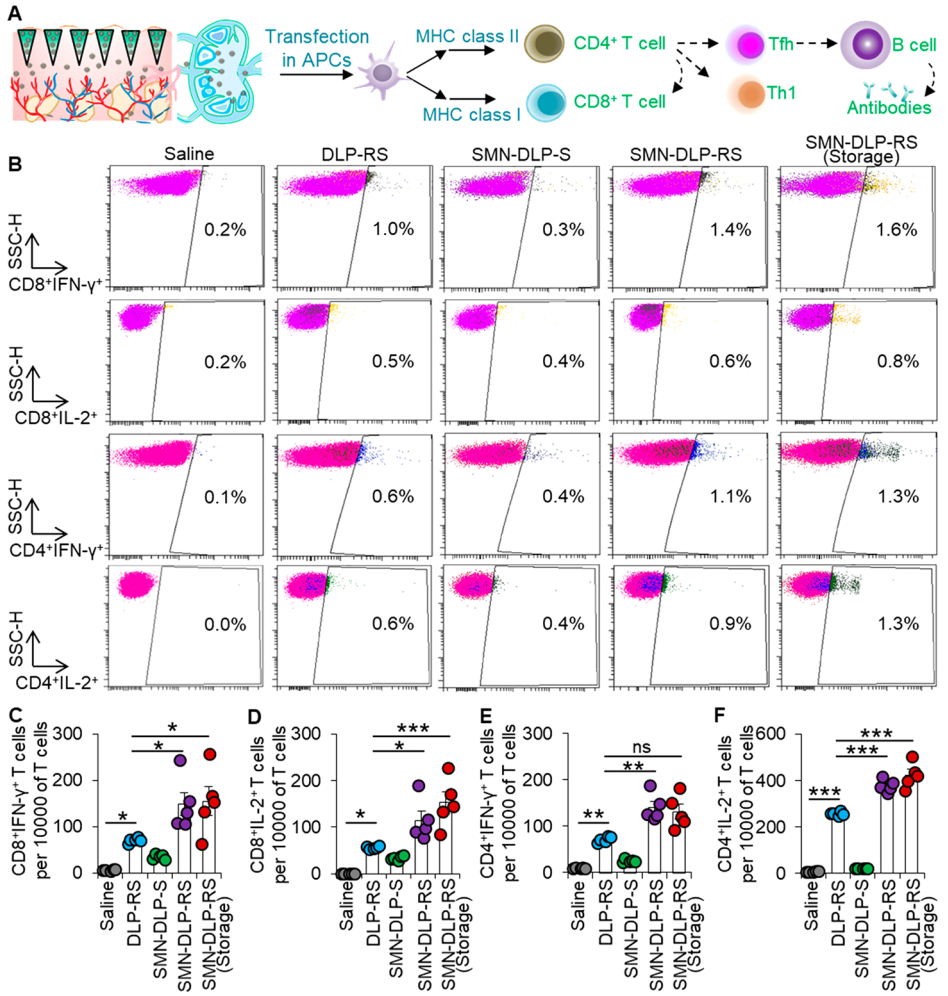

Figure 5. ***In vivo*** **cellular immune responses. (A) A schematic illustration of cellular immune responses after treated mice with SMN-DLP-RS (or RN) patches. (B) Flow cytometry analyses of $CD8^+IFN\text{-}\gamma^+$, $CD8^+IL\text{-}2^+$, $CD4^+IFN\text{-}\gamma^+$, and $CD4^+IL\text{-}2^+$ T cells in splenocytes of mice after treated with saline, DLP-RS, SMN-DLP-S, or SMN-DLP-RS patches (fresh prepared or storage at room temperature for 2 weeks). The dose of R848 and/or pCOV-S is 16.7 and/or 20 μg per mouse, respectively, and mice were sacrificed at day 28 after vaccination. (C−F) The quantitative results of $CD8^+IFN\text{-}\gamma^+$, $CD8^+IL\text{-}2^+$, $CD4^+IFN\text{-}\gamma^+$, and $CD4^+IL\text{-}2^+$ T cells in splenocytes after various treatments. Error bars represent ± s.e.m. (n = 5). ns: not significantly different. *P < 0.05, **P < 0.01, ***P < 0.001 (ANOVA analysis with multiple comparisons).**

Figure S12b, SMN path can penetrate epidermis with a conical cavity, indicating the patch can deliver nanoparticles into the intradermal layer and avoid damaging the nerves and vascular structures. The releasing of nanovaccines was confirmed with Cy5.5-labeled pCOV-S as shown in SI Figure S12c, showing the nanovaccines are observable in the tissue surrounding the microneedle.

To confirm the separable capacity of microneedle, SMN patches were then incubated in water bath (~13 °C) for only 3 min before taking SEM images. Interestingly, all the microneedles were detached from the backing layer and round traces showed the original positions of microneedles (Figure 4G). This capacity is further confirmed with *in vivo* treatment. After manually pressing the SMN patches in the skin of C57BL/6 mice, cold water in a bottle (~13 °C) was attached on the patch for 3 min, and the detached backing layer was collected for SEM imaging. Similarly, all the microneedles were separated from the backing layer as shown in Figure 4H. Those data suggest that the separating layer can be controlled by temperature to quickly separate SMN patch from microneedles with a high efficiency. Of note, this SMN patches are stable in air under cold temperature as there is no liquid to dissolve the PNIPAM-B.

Next, we investigated the biodistribution of injected nanoparticles with IVIS animal imaging. As shown in Figure 4I, most of the DNA vaccines-laden nanoparticles were located at the injection area after 10 min. The fluorescence intensities at treated areas were gradually decreased and almost disappeared after 5 days (120 h, Figure 4I,J). To confirm the released DNA vaccines-laden nanoparticles can migrate to lymph nodes *in vivo*, mice were sacrificed at 24, 72, and 120 h after treated with SMN patches. The lymph nodes were collected for *ex vivo* imaging as shown in Figure 4K,L. The fluorescence of DNA vaccines is evident in the lymph nodes of mice treated with SMN patches after 24 and 72 h. For *ex vivo* imaging of lymph node, we did not observe strong fluorescence after treated with microneedles for 120 h (Figure 4K,L). Considering small molecule dye is not suitable for long-term *in vivo* imaging,[34] nanovaccines may still accumulate in lymph node after 120 h but cannot show strong fluorescence. The targeted delivering capacity to lymph nodes is probably due to two different mechanisms. As illustrated in Figure 1, DNA nanovaccines can be uptake by DCs or other APCs in dermis

https://doi.org/10.1021/acsnano.1c03252
ACS Nano XXXX, XXX, XXX−XXX

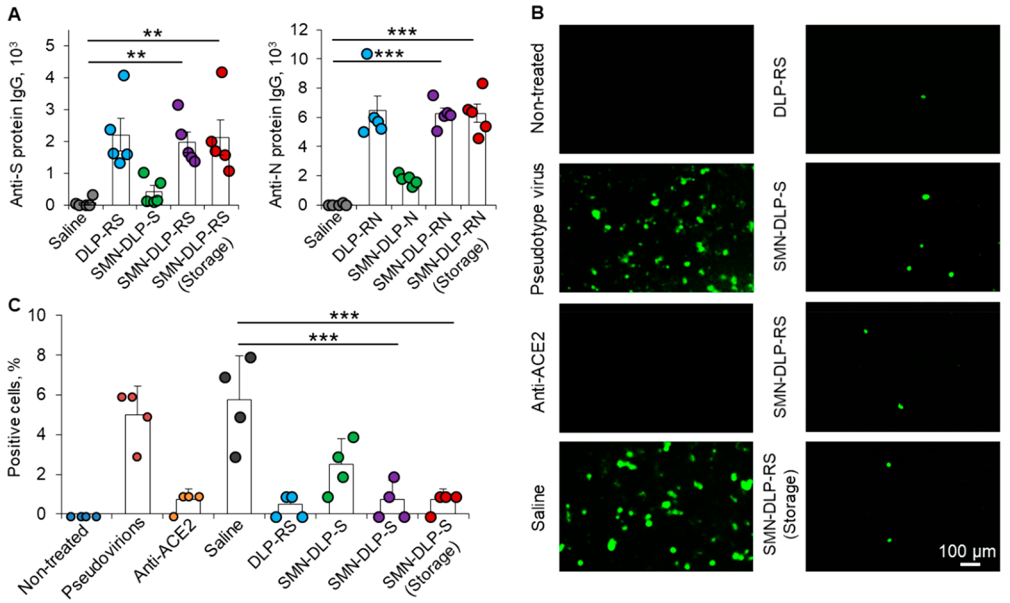

Figure 6. Humoral immune responses to S- and N-proteins in C57BL/6 mice after a single dose of various vaccines. (A) Production level of anti-S protein IgG and anti-N protein IgG in serum (pg/ml) after vaccination for 28 days. Error bars represent ± s.e.m. (n = 5). (B) Typical fluorescence images of GFP (green) in HepG2 cells after treated with GFP expressing SARS-CoV-2 spike pseudotyped virus. The pseudotyped virus can efficiently infected the HepG2 cells but was blocked with anti-ACE2 antibody. Incubation of pseudotyped virus with serums collected from mice (saline, DLP-RS, SMN-DLP-S, SMN-DLP-RS, and SMN-DLP-RS (storage)) was investigated, showing the efficient blocking with DLP-RS and SMN-DLP-RS patches. (C) The quantitative data of GFP-positive cell during each treatment of various groups. Error bars represent ± SD (n = 4). **P < 0.01, ***P < 0.001 (ANOVA analysis with multiple comparison).

layer directly and those matured APCs would migrate to lymph nodes together with nanoparticles. In another way, the released nanovaccines could diffuse into the lymph capillaries and move through the lymph flow to lymph nodes.

The stability of DLP-RS or DLP-RN nanoparticles in SMN patches were investigated by keeping the patches at room temperature for 30 days. The nanoparticles were then collected from the microneedles for further characterizations. As shown in SI Figure S13a, the morphology of DLP-RS or DLP-RN nanoparticles was similar as the fresh prepared nanoparticles (Figure 2B,C). Migration of pCOV-S or pCOV-N in agarose gel indicated that the plasmid was integral during room temperature storage for 30 days compared with fresh prepared plasmid (SI Figure S13b). Importantly, both Western blot and ELISA data confirmed that the stored vaccines could express comparable S- or N-proteins in RAW264.7 and DC2.4 cells (SI Figure S13c,d). Collectively, these results show that the DNA vaccines are stable in microneedles and can be stored at room temperature for at least one month.

***In Vivo* Transfection and Activation of APCs for Immunogenicity.** The adaptive immune system is an important defense against most viral infections. The immunogenicity of DLP-RS or DLP-RN nanoparticles was evaluated in C57BL/6 mice, which were delivered in the dermis layer at back of mice using SMN patches. Since the released DLP-RS or DLP-RN nanoparticles could target the lymph node and present the virus antigen in APCs for humoral and cellular immunity (Figure 5A), the immunocompetent female C57BL/6 mice were immunized with a single dose of DLP-S or DLP-RS-laden SMN patches (SMN-DLP-RS), or intramuscularly injected DLP-RS or DLP-RN nanoparticles. Moreover, to investigate the stability of DNA vaccines-laden SMN patches, the SMN patches stored at room temperature (2 weeks) were also used for vaccination.

$CD4^+$ T cells may differentiate into Tfh, Th1, CD4, or other T cells in response to SARS-CoV-2.[35] Those differentiated T cells can help B cell producing neutralizing antibodies or help CD8 T cell for proliferation or secret cytokines to against virus. $CD8^+$ T cells are important to destroy the virus infected cells. Considering the urgent situation of the COVID-19 pandemic, it is crucial to seek out methods for accelerating, prolonging, and enhancing the immunogenicity of vaccines. We first studied the T cell immune response that was elicited by single doses of immunization of SMN-DLP-RS in mice (20 μg of pCOV-S and 16.7 μg of R848 per mouse). Flow cytometry results showed a significant increase in IFN-γ^+CD8^+ and IL-2^+CD8^+ effector memory T cells in splenocytes from DLP-RS or SMN-DLP-RS vaccinated mice compared with saline group (SI Figure S14 and Figure 5B−D). Interestingly, the percentages of two kinds of T cells are further enhanced after SMN-DLP-RS vaccination, suggesting the better immune response can be achieved by intradermal or lymph node targeted delivery. Those results also indicate that the immunostimulant is important for the efficient vaccination. However, this part is not well studied for current approved SARS-CoV-2 vaccines. In this study, we have included TLRs related adjuvants with DNA vaccines and observed significant immune response for both humoral and cellular immunity, suggesting the immune adjuvants can help the nuclei acid vaccines. It is necessary to systematically investigate the immune response of vaccines after coadministration with adjuvants, such as aluminum, MF59,[36] MPL,[37] AS04,[38] CpG,[39] and others. Especially, it is important to study whether the adjuvants can prolong the immunogenicity of vaccination. More importantly, there is no significant difference between fresh prepared and storage SMN-DLP-RS patches at room temperature (~25 °C) for 2 weeks (SI Figure S14 and Figure 5B−D). Similar as $CD8^+$ T cells, no matter fresh or storage

https://doi.org/10.1021/acsnano.1c03252
ACS Nano XXXX, XXX, XXX−XXX

SMN-DLP-RS can activate the IFN-γ^+CD4$^+$ and IL-2$^+$CD4$^+$ T cells better than intramuscularly injected DLP-RS nanoparticles or SMN-DLP-RS (Figure 5B,E,F). It is worth noting that delivering DLP-RS nanoparticles with SMN patch can induce better immune response than intramuscular injected nanoparticles.

Next, we investigated the SARS-CoV-2 specific T cell immune response upon stimulation with SARS-CoV-2 peptide pools after the vaccination at days 7, 14, 21, and 28. Flow cytometry results showed the SARS-CoV-2 specific IFN-γ^+CD8$^+$ and IL-2$^+$CD8$^+$ effector memory T cells from SMN-DLP-S vaccinated mice were induced at day 7 and became stable after 21 days (SI Figure S15a,b). Importantly, SMN-DLP-RS could induce higher SARS-CoV-2 specific IFN-γ^+CD8$^+$ and IL-2$^+$CD8$^+$ T cells than SMN-DLP-S group, confirming the importance of using immunostimulant (SI Figure S15a,b). Moreover, SARS-CoV-2 specific IFN-γ^+CD4$^+$ and IL-2$^+$CD4$^+$ T cells were also analyzed (SI Figure S15a,b). Unlike CD8$^+$ T cells, the number of IFN-γ^+CD4$^+$ and IL-2$^+$CD4$^+$ T cells were slightly increased in SM-DLP-S vaccinated mice at days 7 and 14. Interestingly, vaccination with SMN-DLP-RS could significantly increase the number of related T cells, suggesting the immunostimulant might be helpful for potential humoral immune response (SI Figure S15a,b).

In consistence with SMN-DLP-RS vaccination, the DLP-RN-laden SMN patches (SMN-DLP-RN) can also efficiently elicit the cellular immune response. As shown in SI Figure S16, IFN-γ and IL-2 positive CD4$^+$ and CD8$^+$ T cells significantly increased after SMN-DLP-RN treatments, and the 2 weeks storage does not significantly affect the immune response. Furthermore, ELISA data showed that secretion of IFN-γ and IL-2 in serum from fresh prepared and storage SMN-DLP-RS or SMN-DLP-RN patches immunized mice is similar and both are significantly higher than normal mice (SI Figure S17). Those data suggest that the N protein may be suitable for developing SARS-CoV-2 vaccine. Collectively, those results demonstrated that the DNA vaccines-laden patches can be storage at room temperature without reducing its immune capacity, which is important for potential storage, transportation, and administration.

We have also determined the humoral immune responses by checking the neutralizing antibodies in serum of the treated mice. As shown in Figure 6A, a single immunization with SMN-DLP-RS or SMN-DLP-RN patch (20 μg of pCOV-S or pCOV-N and 16.7 μg of R848 per mouse) can induce the production of SARS-CoV-2 S- or N-protein specific IgG. The level of S- or N-protein specific IgG is increased after treatment with SMN-DLP-S patches. Moreover, DLP-RS (or RN) and SMN-DLP-RS (or RN) patches can further increase the level of S- or N-protein specific IgG. For DNA immunization, DNA vaccine constructs of S protein may induce high levels of specific binding IgG that showed a balance of IgG1/IgG2a response.[40] Importantly, the storage at room temperature has no effects on the immunogenicity of SMN-DLP-RS (or RN) patches (Figure 6A). Unlike cellular immune response, we did not observe significant increasing of specific IgG between DLP-RS (or RN) nanoparticles and SMN-DLP-RS (or RN) patches treated mice (Figure 6A). However, the SMN-DLP-RS (or RN) patches are much easier and safer for vaccination. It is also worth noting that the immunostimulant (R848) can significantly increase the level of IgG, suggesting the combination of immunostimulant is an important way to enhance the immunogenicity of vaccines.

The duration of SARS-CoV-2 IgG antibodies was determined by checking the IgG titers after vaccinated with SMN-DLP-S or SMN-DLP-RS patch for 7, 14, 21, 28, and 42 days. As shown in SI Figure S18, the IgG antibodies were generated after 14 days and maintained at similar level after 21 days. Similarly, the immunostimulant could significantly increase the IgG titers and keep at similar level for at least 6 weeks. Apart from the antibody presence in the serum, the presence of S protein IgG antibodies in the lungs were also checked as which is important for protection against lower respiratory diseases from virus infection.[41] Unlike serum, S protein IgG antibodies in lung were induced at day 28 or 21 for SMN-DLP-S or SMN-DLP-RS vaccination, respectively (SI Figure S19). Those data suggested that SMN-DLP-RS can potentially provide better protection than SMN-DLP-S vaccination. Of note, the vaccination did not induce IgE isotype antibodies, suggesting that there were no allergic responses in treated mice (SI Figure S20). This is not surprising as PVA or PEI has been widely applied to prepare microneedles or nanoparticles and no allergic responses have been reported.[42,43]

Next, we have applied SARS-CoV-2 spike pseudotyped virus (GFP) to mimic the SARS-CoV-2 virus for cell infection. We first incubated the pseudovirions with HepG2 cells that express angiotensin-converting enzyme 2 (ACE2) as host cells. As shown in Figure 6B,C (for fluorescence images and quantitative results, respectively), the pseudotyped virus can indeed infect the HepG2 cells and express GFP in cells. In contrast, it can be fully blocked if incubated HepG2 cells with anti-ACE2 antibody before pseudovirions treatment, suggesting the pseudotyped virus can enter the cells through ACE2 receptor. Then, we incubated the pseudotyped virus with serum collected from the vaccinated mice and incubated with HepG2 cells to check the infection efficiency. Many cells were infected with pseudotyped virus if incubated with serum from saline group, but can be significantly decreased after incubated with the one from SMN-DLP-S treated mice (Figure 6B,C). In consistence with IgG level, serum from DLP-RS nanoparticles or SMN-DLP-RS patches treated mice shows the best blocking capability and storage of SMN-DLP-RS patches at room temperature does not affect the blocking capability (Figure 6B,C).

Last, the body weights of mice were stable during the 28 days of vaccination with various vaccines (SI Figures S21a and S22a). In addition, there is no obvious damage in the H&E stain of major organs collected from vaccinated mice (SI Figures S21b and S22b). These data suggest the vaccines developed in this study are safe for *in vivo* treatment. Taken together, those results show that SMN-DLP-RS or SMN-DLP-RN vaccine can be stored at room temperature for convenient vaccination and induce high levels of both humoral and cellular immune response against SARS-CoV-2. Meanwhile, we did not include nonhuman primate models in this study to confirm the protection capability of the prepared vaccines. This is because it is extremely difficult to obtain the access to conduct related experiments in the authorized facility.

CONCLUSION

In summary, we developed a tailor-made microneedle-based DNA vaccine to express S- and N-proteins in APCs and trigger the immune responses for blocking the infection of SARS-

https://doi.org/10.1021/acsnano.1c03252
ACS Nano XXXX, XXX, XXX−XXX

CoV-2 virus. The synthesized DA-LPEI amphiphilic polymer can encapsulate the hydrophobic immune adjuvant (R848) and efficiently help the DNA vaccines escaping from the endo/lysosomes without obvious cytotoxicity. To deliver DNA vaccine in APCs-rich area, a separable microneedle patch was applied to deliver those DNA vaccines-laden nanoparticles into the intradermal layer. Taking advantage of the thermoresponsiveness of PNIPAM-B, the backing layer can be easily separated from the patches and leave the microneedle in the intradermal layer for several days. As a result, intradermally delivered DLP-RS or DLP-RN nanovaccines can efficiently activate both humoral and cellular immune response. IFN-γ^+CD4/8$^+$ and IL-2$^+$CD4/8$^+$ effector memory T cells or virus specific IgG are significantly increased after SMN-DLP-RS or SMN-DLP-RN vaccination. Moreover, we further revealed that the SMN-DLP-RS or SMN-DLP-RN vaccine can efficiently induce immune response after storage at room temperature at least for 2 weeks. Ultimately, we did not observe any obvious side effects during the *in vivo* vaccination and serum collected from SMN-DLP-RS vaccinated mice can efficiently protect the HepG2 cells from infecting with SARS-CoV-2 spike pseudotyped virus. This study may lay the foundation for developing a promising thermal stable and easy operating vaccines for combating COVID-19 pandemic.

METHODS

Materials. LPEI (Mw 1.8k), dichloromethane (DCM), and anhydrous tetrahydrofuran (THF) were purchased from Macklin (Shanghai, China). Deoxycholic acid was purchased from 9dingchem Co., Ltd. (Shanghai, China). *N*,*N*′-dicyclohexylcarbodiimide (DCC) and *N*-hydroxysuccinimide (NHS) were purchased from Aladdin (Shanghai, China). R848 and 4′,6-diamidino-2-phenylindole (DAPI) were purchased from MedChemExpress (Monmouth Junction, NJ). Dimethyl sulfoxide-d6 (DMSO-d6), PVA (Mw 85k-124k), and PNIPAM-B were purchased from Sigma-Aldrich (St. Louis, MO). Roswell Park Memorial Institute (RPMI) 1640 medium, penicillin/streptomycin, fetal bovine serum (FBS), PBS, trypsin-EDTA, and dimethyl sulfoxide (DMSO) were purchased from Beyotime (Shanghai, China). Heparin sodium salt, agarose, 1 × TAE buffer, 3-(4,5-dimethyl-2-thiazolyl)-2,5-diphenyl tetrazolium bromide (MTT), Cy5.5-NHS, Lyso-Tracker Green, 4% paraformaldehyde, bicinchoninic acid (BCA) assay kit, SDS-PAGE gel, polyvinylidene difluoride (PVDF), 1 × TBST, defatted milk powder, 3,3′,5,5′-tetramethylbenzidine (TMB), and stop buffer were purchased from Solarbio Science & Technology Co., Ltd. (Beijing, China). GelRed was purchased from Transgen (Beijing, China). Phorbol 12-myristate 13-acetate (PMA), ACK lysing buffer, FcR blocking agent, FITC-anti-CD3 (Biolegend, 100203-1), APC-anti-CD8a (Biolegend, 100712), Pacific blue-anti-IFN-γ antibody (Biolegend, 505817), and PE-Cy7-IL-2 antibody (Biolegend, 503831) were purchased from Dakewe (Beijing, China). IgE, TNF-α, and IL-2 ELISA kit were purchased from MultiSciences (Hangzhou, China). HRP conjugated goat anti-mouse IgG (SA00001−1) and HRP (SA00001-2) conjugated goat anti-rabbit IgG were purchased from Proteintech (Chicago, IL). SARS-CoV-2 nucleocapsid protein ELISA kit, SARS-CoV-2 spike protein ELISA Kit, recombinant SARS-COV-2 nucleocapsid protein, recombinant SARS-COV-2 spike protein, SARS-CoV-2 nucleocapsid rabbit polyclonal antibody (A18797), and SARS-CoV-2 spike rabbit polyclonal antibody (A20137) were purchased from Abclonal Technology (Wuhan, China). SARS-CoV-2 spike pseudotyped virus was purchased from Ji Manchu Biotechnology Co., Ltd. (Shanghai, China). SARS-CoV-2 (spike protein) Peptide Pool was purchased from STEMCELL Technologies China Co., Ltd. (Beijing, China). Polycarbonate microneedle molds were purchased from Laike mold company (Guangzhou, China). All reagents were of analytical grade and used as obtained unless otherwise mentioned.

Plasmids. S-protein and N-protein encoding plasmids were designed and purchased by Fenghui Biotechnology Co., Ltd. (Changsha, China), and their sequences were confirmed by Genewiz (Suzhou, China).

Cells. DC2.4, RAW264.7, and HepG2 cells were supplied by American Type Culture Collection (ATCC, Gaithersburg, MD).

Mice. C57BL/6 mice were purchased from Vital River Laboratory Animal Technology Co. Ltd. (Beijing, China). All mentioned animal experiments in this study were carried out in accordance with the relevant laws and followed the institutional guidelines approved by Institutional Animal Care and Use Committee of National Center for Nanoscience and Technology.

Synthesis of DA-LPEI Conjugate. The DNA vaccines and R848 carrier (DLP) containing cationic and amphiphilic properties was synthesized via the mechanism that the carboxyl groups of deoxycholic acid could be conjugated to the primary amine groups of LPEI according to the previous method.[22,23] Briefly, deoxycholic acid (1.00 g, 2.50 mmol) was activated with DCC (1.55 g, 7.50 mmol) and NHS (0.87 g, 7.50 mmol) in THF at room temperature for 6 h. The activated deoxycholic acid was precipitated in cold *n*-hexane and dried under reduced pressure. Then, the activated deoxycholic acid (0.58 g, 1.50 mmol) dissolved in THF was mixed with LPEI (0.54 g, 0.30 mmol) dissolved in DCM and reacted overnight. This collected product was dried using a rotary evaporator and precipitated in cold acetone, and the precipitate was centrifuged at 4000 rpm for 30 min and dried under air. The product was finally dissolved in deionized water, filtered using Millipore filter 0.8 μm, and lyophilized. The composition of DLP was determined via ^{1}H NMR in DMSO-d6 and FTIR. The obtained molar ratio between DA and LPEI was 4:1.

Synthesis and Characteristics of DLP-RS or DLP-RN Nanovaccines. To encapsulate R848 in DLP nanoparticles, R848 dissolved in ethanol and DLP dissolved in dichloromethane at weight ratio of 1:4 was first mixed and dispersed via sonication until the solution became transparent. The film was obtained when the solvent was completely evaporated using rotary evaporator. Then, the film was homogeneously resuspended in deionized water via sonication. The loading efficiency of R848 in DLP-R is 17.29% ± 0.49%, and its encapsulation efficiency is 83.66% ± 2.85%. To prepare DLP-RS or DLP-RN nanovaccines, pCOV-S (or N) was mixed with the DLP-R cationic nanoparticles synthesized above with a feeding ratio of 1:5 in deionized water and incubated for 30 min at room temperature.

The binding ability of DLP-S or DLP-N was examined by gel electrophoresis. The pDNA (1.0 μg) was first incubated with 1.0, 2.0, or 3.0 μg of DLP nanoparticles at room temperature for 30 min, respectively. Sequentially, the mixtures were loaded on 1% (w/v) agarose gel containing GelStain in 1 × TAE buffer with 6 × loading dye. These gels were allowed to run at 120 V for 20 min in 1 × TAE buffer.

To determine whether DLP-RS or DLP-RN can maintain the stability of pCOV-S or pCOV-N after 30 days, the prepared patchs were stored at room temperature for 30 days and the pCOV-S or pCOV-N in nanoparticles were replaced with heparin competition and collected for further study. Electrophoretic mobility shift assay was conducted with a 1% (w/v) agarose gel at 120 V for 20 min.

The morphology and size of fresh prepared or stored DLP-RS or DLP-RN nanovaccines were imaged with a scanning electron microscope (SEM, S-4800, Hitachi Limited, Tokyo, Japan) and a transmission electron microscopy (TEM, EM200CX; JEOL Ltd., Tokyo, Japan). Briefly, 20 μL of nanovaccines was dropped on a piece of cleaned SEM stub and dried for 12 h under air condition at room temperature. A thin film of Au was then sputter-coated onto the nanovaccines. The quantitative size distribution and zeta potential of DLP-RS or DLP-RN nanovaccines (100 μg/mL in deionized water) were further measured using a dynamic light scattering (Malvern Nano ZS, Malvern, UK).

To determine serum stability, free pCOV-S or pCOV-N or DNA nanovaccines-laden DLP nanoparticles were incubated with PBS containing 20% serum at 37 °C for predetermined time points (0, 6, 12, 24, 36, and 48 h). The DNA vaccines were then replaced with

https://doi.org/10.1021/acsnano.1c03252
ACS Nano XXXX, XXX, XXX−XXX

heparin competition and collected for study. Electrophoretic mobility shift assay was conducted with a 1% (w/v) agarose gel at 120 V for 20 min.

***In Vitro* Cytotoxicity of DLP-RS or DLP-RN Nanovaccines.** DC2.4 and RAW264.7 cells (10 000) were cultured in each well of 96-well plates with 100 μL of medium for 24 h. The cells were then treated with various kinds and concentrations of DLP-RS or DLP-RN nanovaccines for 24 h. MTT solution (20 μL, 5 mg/mL) was added to each well and incubated for 4 h, and replaced with DMSO and incubated for another 1 h. The absorbance at 490 nm was measured by a microplate reader (PerkinElmer, Waltham, MA).

Cellular Uptake and Transfection Efficiency of DLP-RS or DLP-RN Nanovaccines. Cy5.5 labeled pCOV-S (or N) was adopted to track the cellular uptake and cellular distributions. DC2.4 and RAW264.7 cells (2.0×10^5 per well) were cultured on commercial 6-well confocal plate with 2.0 mL of cell culture medium for 24 h. Then cells were washed with PBS and incubated with free pCOV-S, DLP-RS or DLP-RN nanovaccines for 2, 4, and 6 h. Then, cells were washed with PBS for three times and stained using DAPI for 10 min and Lyso-Tracker (green) for 30 min before being fixed with 4% Paraformaldehyde Fix Solution (PFA). The cells were exhibited and imaged using a Zeiss LSM 880 confocal laser scanning microscope (München, Germany). Regarding flow cytometry, the cells were washed with PBS for three times and analyzed by a flow cytometer (LSRFortessa, Becton Dickinson, Franklin Lakes, NJ), and data were analyzed via FlowJo software (TreeStar, Ashland, OR).

For S- and N-protein expression, DC2.4 and RAW264.7 cells (2.0×10^5 per well) were cultured in 6-well plates for 24 h. Then, the cells were treated with free pCOV-S, free pCOV-N, fresh prepared DLP-RS, DLP-S, DLP-RN, DLP-N, storage DLP-RS, or storage DLP-RN for another 48 h. Cells in each well were then treated with 200 μL of 1 × cell lysis buffer and cell fragments were removed by centrifugation at 12000 rpm for 10 min. The total protein concentration was analyzed using a BCA assay kit. The expression of S- and N-proteins were confirmed by Western blot analysis and ELISA. In detail, the proteins were loaded on a 10% SDS-PAGE gel with electrophoresis at 80 V for 90 min. Then, the proteins in gel were transferred to PVDF membrane and blocked with 5% skim milk in 1 × TBST buffer at room temperature for 1 h, incubated with diluted each kind of primary antibody (1:2000) from rabbit in 5% skim milk in 1 × TBST buffer at 4 °C overnight. After washing with 1× TBST, the membrane was incubated with HRP-conjugated goat anti-rabbit secondary antibody (1:5000) at room temperature for 1 h. The quantitative measurements of them were, respectively, evaluated using SARS-CoV-2 nucleocapsid protein ELISA kit and SARS-CoV-2 spike protein ELISA Kit according to the manufacture's instruction.

Fabrication and Characteristics of SMN Patches. PVA polymers were used to fabricate the microneedle layer via a micromolding technology.[44] 20 wt % of PVA solution was uniformly mixed with the desired DLP-RS or DLP-RN nanovaccines that contained 20 μg of pCOV-S (or N) and 16.7 μg of R848 and carefully added into all microcavities. After removed the bubbles, microneedles were dried at room temperature for at least 10 h. Thereafter, 50 μL of 5% cold PNIPAM solution was uniformly plated onto the flat cavity of the mold and then dried at room temperature for 2 h, which would be regarded as the separable layer. In order to form the back layer, 50 μL of 20 wt % pure PVA solution was also uniformly plated onto the dried PNIPAM film. Bubbles in this PVA solution was also removed via the vacuum evaporation at a pressure of −20 kPa for 5 min, and this back-layer solution was dried under air condition at room temperature for additional 10 h to construct a combined film containing both separable layer and back layer. After the SMN patches were completely fabricated, it could be gently detached from the mold via an adhesive tape. The morphologies of MNs with/without DNA nanovaccines were observed using a SEM mentioned above, and the morphologies of MNs with Cy5.5-DNA nanovaccines and MNs without Cy5.5-DNA nanovaccines but with FITC mixed separating layer were photographed using a fluorescence microscope (Nikon, Irvine, CA, USA) and a ChemiDoc Touch Imaging System (Biorad, Hercules, CA).

To prove the skin penetration capability of SMN patches *in vivo*, a piece of MNs patch that encapsulated FITC in its microneedle layer was inserted onto the bare skin at an application force of 2 N. After removed the back layer, the skin was subsequently imaged using a ChemiDoc Tough Imaging System. The holes and damages in the epidermis were clearly confirmed via H&E staining.

To prove the diffusion of DNA nanovaccines in the epidermis from SMN patches, a piece of SMN patch containing Cy5.5-DNA nanovaccines was inserted into the bare skin of a 6-week old C57BL/6 female mouse at an application force of 2 N. After removing the back layer with cold water, the section of this piece of skin was observed via a fluorescence microscope (Nikon, Irvine, CA).

To track intradermal delivery, lymphatic delivery, and clearance of DNA nanovaccines, SMN with Cy5.5-DNA nanovaccines was cutaneously injected into the bare skin of 6-week age C57BL/6 female mice. Their backs were imaged and quantified at predetermined time points (10 min, 24, 48, 72, and 120 h), and the collected lymph nodes were imaged and quantified at predetermined time points (24, 72, and 120 h) via IVIS *in vivo* imaging system (PerkinElmer, Waltham, MA, USA).

***In Vivo* Animal Study.** All animal experiments in this study were performed in accordance with the relevant rules and regulations approved by Institutional Animal Care and Use Committee of National Center for Nanoscience and Technology. To carry out *in vivo* vaccinations, SMN-DLP-RS (or RN) patches were inserted onto the absolutely bare skin of each 6-week old C57BL/6 female mouse (20 μg of pCOV-S or pCOV-N and 16.7 μg of R848) at an application force of 2 N. Next, the suitable cold water in bottle (∼13 °C) was applied and attached to the patches. After 3 min, the backing layer was removed. All the mice were sacrificed on day 28, and the serum and spleens were collected for the following studies. The major organs were collected for H&E staining.

Humoral Immunity. Serum samples were collected 7 days, 14 days, 21 days, 28 days, and 42 days after vaccination, and levels of antibodies were detected by ELISA. Regarding levels of anti-S or anti-N protein antibody, S- or N-protein was diluted into 10 μg/mL in antigen-coated buffer (8.4 g $NaHCO_3$ in 1000 mL of deionized water, pH 9.0) and coated in a 96-well microplate at 4 °C overnight. After rinsing twice with PBST buffer, the plates were incubated with blocking solution (5% nonfat dry milk in phosphate buffered saline with 1% Tween 20 in PBST) for 1 h at 37 °C. Next, the plates were incubated with serum samples at 1:10 dilution in blocking solution and 100 μL of HRP conjugated goat anti-mouse IgG at 1:5000 dilution at 37 °C for 1 h. After washing three times with PBST, 100 μL of TMB substrate was added to each well, and the color was changed after 15 min. Finally, the reaction was stopped after adding 100 μL of 2 M H_2SO_4 per well. The absorbance was read at 450 nm by a microplate reader (PerkinElmer, Waltham, MA). Levels of IgE, INF-γ and IL-2 were directly evaluated via MultiSciences ELISA kits according to the manufacturers.

Cellular Immunity. Spleens were collected 7 days, 14 days, 21 days, and 28 days after vaccination. ACK lysing buffer was used for clearing red cells and isolating splenocytes. Splenocytes were then activated in culture medium containing 5 μg/mL of PMA or 5 μg/mL of SARS-CoV-2 (spike protein) Peptide Pool for 6 h. The collected cells were first blocked with FcR blocking agent and stained with surface markers FITC-anti-CD3 (1:100 dilution), PE-anti-CD4 (1:100 dilution), and APC-anti-CD8a (1:100 dilution) antibodies before being fixed, permeabilized, and incubated with Pacific blue-anti-IFN-γ (1:100 dilution) and PE-Cy7-anti-IL-2 antibody (1:100 dilution). Finally, the cells were washed with PBS two times and analyzed by a flow cytometer (LSRFortessa, Becton Dickinson, Franklin Lakes, NJ, USA), and data were analyzed via FlowJo software (TreeStar, Ashland, OR).

Pseudovirus Model. HepG2 cells expressing ACE2 receptors were cultured in 96-well plates for 24 h. Various kinds of diluted serum samples (10 times) that were collected from mice above were mixed with diluted GFP expressing SARS-CoV-2 spike pseudotyped virus at a final concentration of 1 μg/mL according to the manufacturers and incubated at 37 °C for 1 h. The cells were then

https://doi.org/10.1021/acsnano.1c03252
ACS Nano XXXX, XXX, XXX−XXX

treated with various kinds of mixtures and incubated for 24 h. Finally, GFP signals from cells were observed and imaged via a fluorescent microscopy.

Statistical Analysis. All data are reported as mean ± standard deviation (SD) or SEM as indicated. The ANOVA analyses were used to assess two-group differences with multiple comparison tests. In all cases, a *p*-value less than 0.05 was considered to be statistically significant.

Data Availability. All data supporting the findings of this study are available from the corresponding authors upon request.

ASSOCIATED CONTENT

Supporting Information

The Supporting Information is available free of charge at https://pubs.acs.org/doi/10.1021/acsnano.1c03252.

^{1}H NMR and FTIR spectra of DA-LPEI polymer; structure of plasmids encoding S- and N-protein; zeta potential, cytotoxicity, cellular uptake of prepared nanoparticles; cellular uptake, transfection and virus antigen of free plasmid in cells; Fabrication process, skin penetration capability of SMN patch; characterizations of DLP-RS and DLP-RN nanoparticles in SMN patch; gating strategy used for the flow cytometry; SARS-CoV-2 specific cellular immune responses, humoral immune response and cytokine secretion after treatment; body weight and H&E staining of major organs (PDF)

AUTHOR INFORMATION

Corresponding Authors

Guangjun Nie − *CAS Key Laboratory for Biomedical Effects of Nanomaterials & Nanosafety, CAS Center for Excellence in Nanoscience, National Center for Nanoscience and Technology, Beijing 100190, China; University of Chinese Academy of Sciences, Beijing 100049, China;* orcid.org/0000-0001-5040-9793; Email: niegj@nanoctr.cn

Hui Li − *Dongfang Hospital, Beijing University of Chinese Medicine, Beijing 100078, China*; Email: lihui8832@163.com

Hai Wang − *CAS Key Laboratory for Biomedical Effects of Nanomaterials & Nanosafety, CAS Center for Excellence in Nanoscience, National Center for Nanoscience and Technology, Beijing 100190, China; University of Chinese Academy of Sciences, Beijing 100049, China;* orcid.org/0000-0002-1292-998X; Email: wanghai@nanoctr.cn

Authors

Yue Yin − *CAS Key Laboratory for Biomedical Effects of Nanomaterials & Nanosafety, CAS Center for Excellence in Nanoscience, National Center for Nanoscience and Technology, Beijing 100190, China*

Wen Su − *CAS Key Laboratory for Biomedical Effects of Nanomaterials & Nanosafety, CAS Center for Excellence in Nanoscience, National Center for Nanoscience and Technology, Beijing 100190, China*

Jie Zhang − *CAS Key Laboratory for Biomedical Effects of Nanomaterials & Nanosafety, CAS Center for Excellence in Nanoscience, National Center for Nanoscience and Technology, Beijing 100190, China*

Wenping Huang − *CAS Key Laboratory for Biomedical Effects of Nanomaterials & Nanosafety, CAS Center for Excellence in Nanoscience, National Center for Nanoscience and Technology, Beijing 100190, China*

Xiaoyang Li − *CAS Key Laboratory for Biomedical Effects of Nanomaterials & Nanosafety, CAS Center for Excellence in Nanoscience, National Center for Nanoscience and Technology, Beijing 100190, China; Department of Orthopedics, National Cancer Center/National Clinical Research Center for Cancer/Cancer Hospital, Chinese Academy of Medical Sciences and Peking Union Medical College, Beijing 100021, China*

Haixia Ma − *CAS Key Laboratory for Biomedical Effects of Nanomaterials & Nanosafety, CAS Center for Excellence in Nanoscience, National Center for Nanoscience and Technology, Beijing 100190, China*

Mixiao Tan − *CAS Key Laboratory for Biomedical Effects of Nanomaterials & Nanosafety, CAS Center for Excellence in Nanoscience, National Center for Nanoscience and Technology, Beijing 100190, China*

Haohao Song − *CAS Key Laboratory for Biomedical Effects of Nanomaterials & Nanosafety, CAS Center for Excellence in Nanoscience, National Center for Nanoscience and Technology, Beijing 100190, China*

Guoliang Cao − *CAS Key Laboratory for Biomedical Effects of Nanomaterials & Nanosafety, CAS Center for Excellence in Nanoscience, National Center for Nanoscience and Technology, Beijing 100190, China*

Shengji Yu − *Department of Orthopedics, National Cancer Center/National Clinical Research Center for Cancer/Cancer Hospital, Chinese Academy of Medical Sciences and Peking Union Medical College, Beijing 100021, China*

Di Yu − *Department of Immunology, Genetics and Pathology, Science for Life Laboratory, Uppsala University, Uppsala 75185, Sweden*

Ji Hoon Jeong − *School of Pharmacy, Sungkyunkwan University, Suwon 16419, Republic of Korea;* orcid.org/0000-0002-4836-3551

Xiao Zhao − *CAS Key Laboratory for Biomedical Effects of Nanomaterials & Nanosafety, CAS Center for Excellence in Nanoscience, National Center for Nanoscience and Technology, Beijing 100190, China*

Complete contact information is available at: https://pubs.acs.org/10.1021/acsnano.1c03252

Notes

The authors declare no competing financial interest.

ACKNOWLEDGMENTS

This work was financially supported by NSFC (31971307, 32000950) and the Key Laboratory of Biomedical Effects of Nanomaterials and Nanosafety, CAS (NSKF202009).

REFERENCES

(1) WHO Coronavirus (COVID-19) Dashboard. https://covid19.who.int/ (accessed 2021/3/23).

(2) Corey, L.; Mascola, J. R.; Fauci, A. S.; Collins, F. S. A Strategic Approach to COVID-19 Vaccine R&D. *Science* **2020**, *368*, 948−950.

(3) Lutz, H.; Popowski, K. D.; Dinh, P. U. D.; Cheng, K. Advanced Nanobiomedical Approaches to Combat Coronavirus Disease of 2019. *Adv. Biomed. Res.* **2021**, *1*, 20000632021.

(4) Popowski, K. D.; Dinh, P. U. D.; George, A.; Lutz, H.; Cheng, K. Exosome Therapeutics for COVID-19 and Respiratory Viruses. *View* **2021**, *2*, 20200186202.

(5) Banerji, A.; Wickner, P. G.; Saff, R.; Stone, C. A., Jr; Robinson, L. B.; Long, A. A.; Wolfson, A. R.; Williams, P.; Khan, D. A.; Phillips, E.; Blumenthal, K. G. mRNA Vaccines to Prevent COVID-19 Disease

and Reported Allergic Reactions: Current Evidence and Suggested Approach. *J. Allergy Clin. Immunol.* **2021**, *9*, 1423−1437.
(6) Crommelin, D. J. A.; Anchordoquy, T. J.; Volkin, D. B.; Jiskoot, W.; Mastrobattista, E. Addressing the Cold Reality of mRNA Vaccine Stability. *J. Pharm. Sci.* **2021**, *110*, 997−1001.
(7) Eyawo, O.; Viens, A. M.; Ugoji, U. C. Lockdowns and Low- and Middle-Income Countries: Building a Feasible, Effective, and Ethical COVID-19 Response Strategy. *Global Health* **2021**, *17*, 13.
(8) Xiao, K.; Zhai, J.; Feng, Y.; Zhou, N.; Zhang, X.; Zou, J. J.; Li, N.; Guo, Y.; Li, X.; Shen, X.; Zhang, Z.; Shu, F.; Huang, W.; Li, Y.; Zhang, Z.; Chen, R. A.; Wu, Y. J.; Peng, S. M.; Huang, M.; Xie, W. J.; et al. Isolation of SARS-CoV-2-Related Coronavirus from Malayan Pangolins. *Nature* **2020**, *583*, 286−289.
(9) Volz, E.; Hill, V.; McCrone, J. T.; Price, A.; Jorgensen, D.; O'Toole, A.; Southgate, J.; Johnson, R.; Jackson, B.; Nascimento, F. F.; Rey, S. M.; Nicholls, S. M.; Colquhoun, R. M.; da Silva Filipe, A.; Shepherd, J.; Pascall, D. J.; Shah, R.; Jesudason, N.; Li, K.; Jarrett, R.; et al. Evaluating the Effects of SARS-CoV-2 Spike Mutation D614G on Transmissibility and Pathogenicity. *Cell* **2021**, *184*, 64−75.
(10) Walls, A. C.; Park, Y. J.; Tortorici, M. A.; Wall, A.; McGuire, A. T.; Veesler, D. Structure, Function, and Antigenicity of the SARS-CoV-2 Spike Glycoprotein. *Cell* **2020**, *183*, 1735.
(11) Du, L.; He, Y.; Jiang, S.; Zheng, B. J. Development of Subunit Vaccines against Severe Acute Respiratory Syndrome. *Drugs Today* **2008**, *44*, 63−73.
(12) Dai, W.; Zhang, B.; Jiang, X. M.; Su, H.; Li, J.; Zhao, Y.; Xie, X.; Jin, Z.; Peng, J.; Liu, F.; Li, C.; Li, Y.; Bai, F.; Wang, H.; Cheng, X.; Cen, X.; Hu, S.; Yang, X.; Wang, J.; Liu, X.; et al. Structure-Based Design of Antiviral Drug Candidates Targeting the SARS-CoV-2 Main Protease. *Science* **2020**, *368*, 1331−1335.
(13) Auvinen, H.; Zhang, H.; Nonappa Kopilow, A.; Niemela, E. H.; Nummelin, S.; Correia, A.; Santos, H. A.; Linko, V.; Kostiainen, M. A. Protein Coating of DNA Nanostructures for Enhanced Stability and Immunocompatibility. *Adv. Healthcare Mater.* **2017**, *6*, 6.
(14) Duong, H. T. T.; Yin, Y.; Thambi, T.; Nguyen, T. L.; Giang Phan, V. H.; Lee, M. S.; Lee, J. E.; Kim, J.; Jeong, J. H.; Lee, D. S. Smart Vaccine Delivery Based on Microneedle Arrays Decorated with Ultra-pH-Responsive Copolymers for Cancer Immunotherapy. *Biomaterials* **2018**, *185*, 13−24.
(15) Duong, H. T. T.; Kim, N. W.; Thambi, T.; Giang Phan, V. H.; Lee, M. S.; Yin, Y.; Jeong, J. H.; Lee, D. S. Microneedle Arrays Coated with Charge Reversal pH-Sensitive Copolymers Improve Antigen Presenting Cells-Homing DNA Vaccine Delivery and Immune Responses. *J. Controlled Release* **2018**, *269*, 225−234.
(16) Ball, R. L.; Bajaj, P.; Whitehead, K. A. Achieving Long-Term Stability of Lipid Nanoparticles: Examining the Effect of pH, Temperature, and Lyophilization. *Int. J. Nanomed.* **2017**, *12*, 305−315.
(17) McMahan, K.; Yu, J.; Mercado, N. B.; Loos, C.; Tostanoski, L. H.; Chandrashekar, A.; Liu, J.; Peter, L.; Atyeo, C.; Zhu, A.; Bondzie, E. A.; Dagotto, G.; Gebre, M. S.; Jacob-Dolan, C.; Li, Z.; Nampanya, F.; Patel, S.; Pessaint, L.; Van Ry, A.; Blade, K.; et al. Correlates of Protection against SARS-CoV-2 in Rhesus Macaques. *Nature* **2021**, *590*, 630−634.
(18) Hsu, J. P.; Phoon, M. C.; Koh, G. C.; Chen, M. I.; Lee, V. J.; Wu, Y.; Xie, M. L.; Cheong, A.; Leo, Y. S.; Chow, V. T. Comparison of Neutralizing Antibody and Cell-Mediated Immune Responses to Pandemic H1N1 2009 Influenza Virus before and after H1N1 2009 Influenza Vaccination of Elderly Subjects and Healthcare Workers. *Int. J. Infect. Dis.* **2012**, *16*, No. e621−7.
(19) Cockburn, J. J.; Navarro Sanchez, M. E.; Fretes, N.; Urvoas, A.; Staropoli, I.; Kikuti, C. M.; Coffey, L. L.; Arenzana Seisdedos, F.; Bedouelle, H.; Rey, F. A. Mechanism of Dengue Virus Broad Cross-Neutralization by a Monoclonal Antibody. *Structure* **2012**, *20*, 303−14.
(20) Grifoni, A.; Weiskopf, D.; Ramirez, S. I.; Mateus, J.; Dan, J. M.; Moderbacher, C. R.; Rawlings, S. A.; Sutherland, A.; Premkumar, L.; Jadi, R. S.; Marrama, D.; de Silva, A. M.; Frazier, A.; Carlin, A. F.; Greenbaum, J. A.; Peters, B.; Krammer, F.; Smith, D. M.; Crotty, S.; Sette, A. Targets of T Cell Responses to SARS-CoV-2 Coronavirus in Humans with COVID-19 Disease and Unexposed Individuals. *Cell* **2020**, *181*, 1489−1501.
(21) Kim, N. W.; Kim, S. Y.; Lee, J. E.; Yin, Y.; Lee, J. H.; Lim, S. Y.; Kim, E. S.; Duong, H. T. T.; Kim, H. K.; Kim, S.; Kim, J. E.; Lee, D. S.; Kim, J.; Lee, M. S.; Lim, Y. T.; Jeong, J. H. Enhanced Cancer Vaccination by *in Situ* Nanomicelle-Generating Dissolving Microneedles. *ACS Nano* **2018**, *12*, 9702−9713.
(22) Moon, H. H.; Joo, M. K.; Mok, H.; Lee, M.; Hwang, K. C.; Kim, S. W.; Jeong, J. H.; Choi, D.; Kim, S. H. MSC-Based VEGF Gene Therapy in Rat Myocardial Infarction Model Using Facial Amphipathic Bile Acid-Conjugated Polyethyleneimine. *Biomaterials* **2014**, *35*, 1744−1754.
(23) Kim, D.; Hong, J.; Moon, H. H.; Nam, H. Y.; Mok, H.; Jeong, J. H.; Kim, S. W.; Choi, D.; Kim, S. H. Anti-Apoptotic Cardioprotective Effects of SHP-1 Gene Silencing against Ischemia-Reperfusion Injury: Use of Deoxycholic Acid-Modified Low Molecular Weight Polyethyleneimine as a Cardiac siRNA-Carrier. *J. Controlled Release* **2013**, *168*, 125−134.
(24) Babiuk, S.; Baca-Estrada, M.; Babiuk, L. A.; Ewen, C.; Foldvari, M. Cutaneous Vaccination: The Skin as an Immunologically Active Tissue and the Challenge of Antigen Delivery. *J. Controlled Release* **2000**, *66*, 199−214.
(25) Zaric, M.; Lyubomska, O.; Touzelet, O.; Poux, C.; Al-Zahrani, S.; Fay, F.; Wallace, L.; Terhorst, D.; Malissen, B.; Henri, S.; Power, U. F.; Scott, C. J.; Donnelly, R. F.; Kissenpfennig, A. Skin Dendritic Cell Targeting *via* Microneedle Arrays Laden with Antigen-Encapsulated Poly-D, L-Lactide-Co-Glycolide Nanoparticles Induces Efficient Antitumor and Antiviral Immune Responses. *ACS Nano* **2013**, *7*, 2042−55.
(26) Jere, D.; Jiang, H. L.; Arote, R.; Kim, Y. K.; Choi, Y. J.; Cho, M. H.; Akaike, T.; Cho, C. S. Degradable Polyethylenimines as DNA and Small Interfering RNA Carriers. *Expert Opin. Drug Delivery* **2009**, *6*, 827−34.
(27) Wang, H.; Zhao, Y.; Wu, Y.; Hu, Y. L.; Nan, K.; Nie, G.; Chen, H. Enhanced Anti-Tumor Efficacy by Co-Delivery of Doxorubicin and Paclitaxel with Amphiphilic Methoxy PEG-PLGA Copolymer Nanoparticles. *Biomaterials* **2011**, *32*, 8281−90.
(28) Taranejoo, S.; Chandrasekaran, R.; Cheng, W.; Hourigan, K. Bioreducible PEI-Functionalized Glycol Chitosan: A Novel Gene Vector with Reduced Cytotoxicity and Improved Transfection Efficiency. *Carbohydr. Polym.* **2016**, *153*, 160−168.
(29) Pathak, A.; Kumar, P.; Chuttani, K.; Jain, S.; Mishra, A. K.; Vyas, S. P.; Gupta, K. C. Gene Expression, Biodistribution, and Pharmacoscintigraphic Evaluation of Chondroitin Sulfate-PEI Nanoconstructs Mediated Tumor Gene Therapy. *ACS Nano* **2009**, *3*, 1493−505.
(30) Carli, G.; Nichele, I.; Ruggeri, M.; Barra, S.; Tosetto, A. Deep Vein Thrombosis (DVT) Occurring Shortly after the Second Dose of mRNA SARS-CoV-2 Vaccine. *Intern Emerg Med.* **2021**, *16*, 803−804.
(31) Li, W.; Terry, R. N.; Tang, J.; Feng, M. R.; Schwendeman, S. P.; Prausnitz, M. R. Rapidly Separable Microneedle Patch for the Sustained Release of a Contraceptive. *Nat. Biomed. Eng.* **2019**, *3*, 220−229.
(32) Chu, L. Y.; Prausnitz, M. R. Separable Arrowhead Microneedles. *J. Controlled Release* **2011**, *149*, 242−249.
(33) Jung, C. R.; Lahiji, S. F.; Kim, Y.; Kim, H.; Jung, H. Rapidly Separable Micropillar Integrated Dissolving Microneedles. *Pharmaceutics* **2020**, *12*, 581.
(34) Aitken, C. E.; Marshall, R. A.; Puglisi, J. D. An Oxygen Scavenging System for Improvement of Dye Stability in Single-Molecule Fluorescence Experiments. *Biophys. J.* **2008**, *94*, 1826−1835.
(35) Kang, Y. F.; Sun, C.; Zhuang, Z.; Yuan, R. Y.; Zheng, Q.; Li, J. P.; Zhou, P. P.; Chen, X. C.; Liu, Z.; Zhang, X.; Yu, X. H.; Kong, X. W.; Zhu, Q. Y.; Zhong, Q.; Xu, M.; Zhong, N. S.; Zeng, Y. X.; Feng, G. K.; Ke, C.; Zhao, J. C.; et al. Rapid Development of SARS-CoV-2 Spike Protein Receptor-Binding Domain Self-Assembled Nanoparticle Vaccine Candidates. *ACS Nano* **2021**, *15*, 2738−2752.

https://doi.org/10.1021/acsnano.1c03252
ACS Nano XXXX, XXX, XXX−XXX

(36) Ko, E. J.; Kang, S. M. Immunology and Efficacy of MF59-Adjuvanted Vaccines. *Hum. Vaccines Immunother.* **2018**, *14*, 3041−3045.
(37) Cluff, C. W. Monophosphoryl Lipid A (MPL) as an Adjuvant for Anti-Cancer Vaccines: Clinical Results. *Adv. Exp. Med. Biol.* **2009**, *667*, 111−123.
(38) Didierlaurent, A. M.; Morel, S.; Lockman, L.; Giannini, S. L.; Bisteau, M.; Carlsen, H.; Kielland, A.; Vosters, O.; Vanderheyde, N.; Schiavetti, F.; Larocque, D.; Van Mechelen, M.; Garçon, N. AS04, an Aluminum Salt- and TLR4 Agonist-Based Adjuvant System, Induces a Transient Localized Innate Immune Response Leading to Enhanced Adaptive Immunity. *J. Immunol.* **2019**, *183*, 6186−6197.
(39) Bode, C.; Zhao, G.; Steinhagen, F.; Kinjo, T.; Klinman, D. M. CpG DNA as a Vaccine Adjuvant. *Expert Rev. Vaccines* **2011**, *10*, 499−511.
(40) Prompetchara, E.; Ketloy, C.; Tharakhet, K.; Kaewpang, P.; Buranapraditkun, S.; Techawiwattanaboon, T.; Sathean-Anan-Kun, S.; Pitakpolrat, P.; Watcharaplueksadee, S.; Phumiamorn, S.; Wijagkanalan, W.; Patarakul, K.; Palaga, T.; Ruxrungtham, K. DNA Vaccine Candidate Encoding SARS-CoV-2 Spike Proteins Elicited Potent Humoral and Th1 Cell-Mediated Immune Responses in Mice. *PLoS One* **2021**, *16*, No. e0248007.
(41) Perlman, S.; Dandekar, A. A. Immunopathogenesis of Coronavirus Infections: Implications for SARS. *Nat. Rev. Immunol.* **2005**, *5*, 917−927.
(42) Ahmed Saeed Al-Japairai, K.; Mahmood, S.; Hamed Almurisi, S.; Reddy Venugopal, J.; Rebhi Hilles, A.; Azmana, M.; Raman, S. Current Trends in Polymer Microneedle for Transdermal Drug Delivery. *Int. J. Pharm.* **2020**, *587*, 119673.
(43) Chen, Z.; Lv, Z.; Sun, Y.; Chi, Z.; Qing, G. Recent Advancements in Polyethyleneimine-Based Materials and Their Biomedical, Biotechnology, and Biomaterial Applications. *J. Mater. Chem. B* **2020**, *8*, 2951−2973.
(44) Chu, L. Y.; Choi, S. O.; Prausnitz, M. R. Fabrication of Dissolving Polymer Microneedles for Controlled Drug Encapsulation and Delivery: Bubble and Pedestal Microneedle Designs. *J. Pharm. Sci.* **2010**, *99*, 4228−4238.

https://doi.org/10.1021/acsnano.1c03252
ACS Nano XXXX, XXX, XXX−XXX